ON-LINE SUPPLEMENT TO

NOS1AP polymorphisms reduce NOS1 activity and interact with prolonged repolarization in arrhythmogenesis

C Ronchi et al.

SUPPLEMENT FIGURES

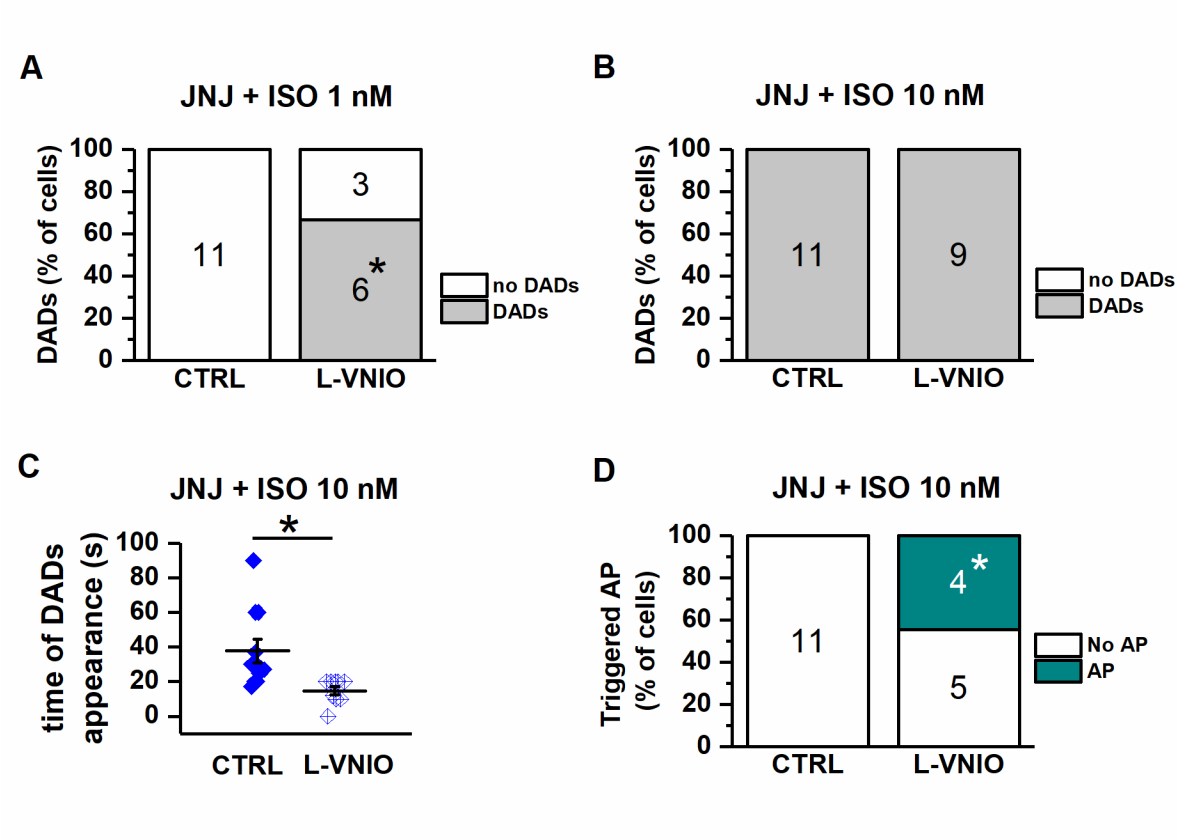

Figure S1. Effect of NOS1 inhibition by L-VNIO on DADs incidence and properties in GP myocytes with a LQT1 background. L-VNIO was tested in the presence of I_{Ks} blockade and β-adrenergic stimulation (by 1 and 10 nM ISO); A) DADs incidence at 1 nM ISO in CTRL and L-VNIO; B) DADs incidence at 10 nM ISO in CTRL and L-VNIO; C) Time of DADs onset after repolarization at 10 nM ISO in CTRL and L-VNIO; D) Incidence of triggered APs at 10 nM ISO in CTRL and L-VNIO. Sample sizes: CTRL n=11/4, L-VNIO n=9/3 for all panels. *=*P*<0.05 vs CTRL from unpaired Student's test and chi squared test.

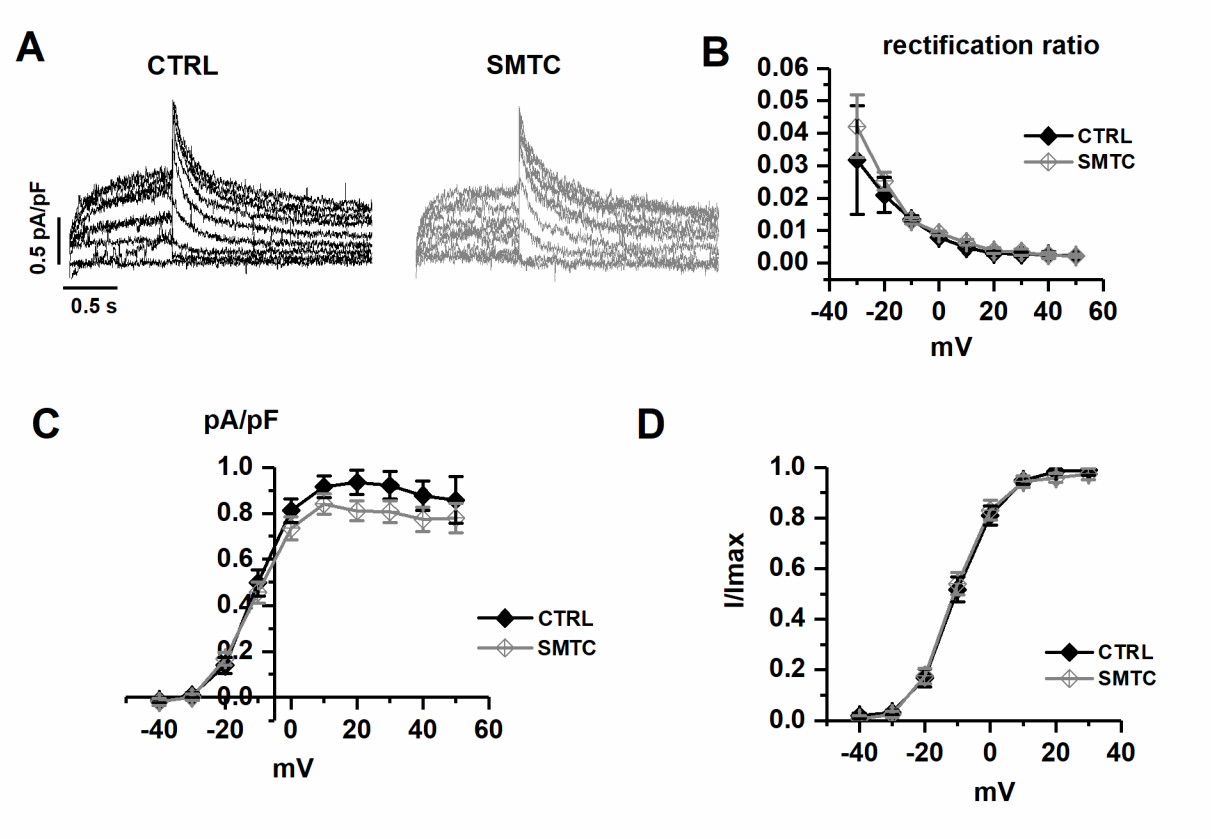

Figure S2. Effect of NOS1 inhibition on I_{Kr}. Data for CTRL and SMTC are presented in each panel. A) Records of I_{Kr} during step and tail at different step voltages; B) V-dependency of I_{Kr} rectification ratio (inactivation). C) I/V relationships of I_{Kr} tail current density; D) I_{Kr} activation curve. Sample sizes: CTRL n=14/5, SMTC n=23/5 for all panels.

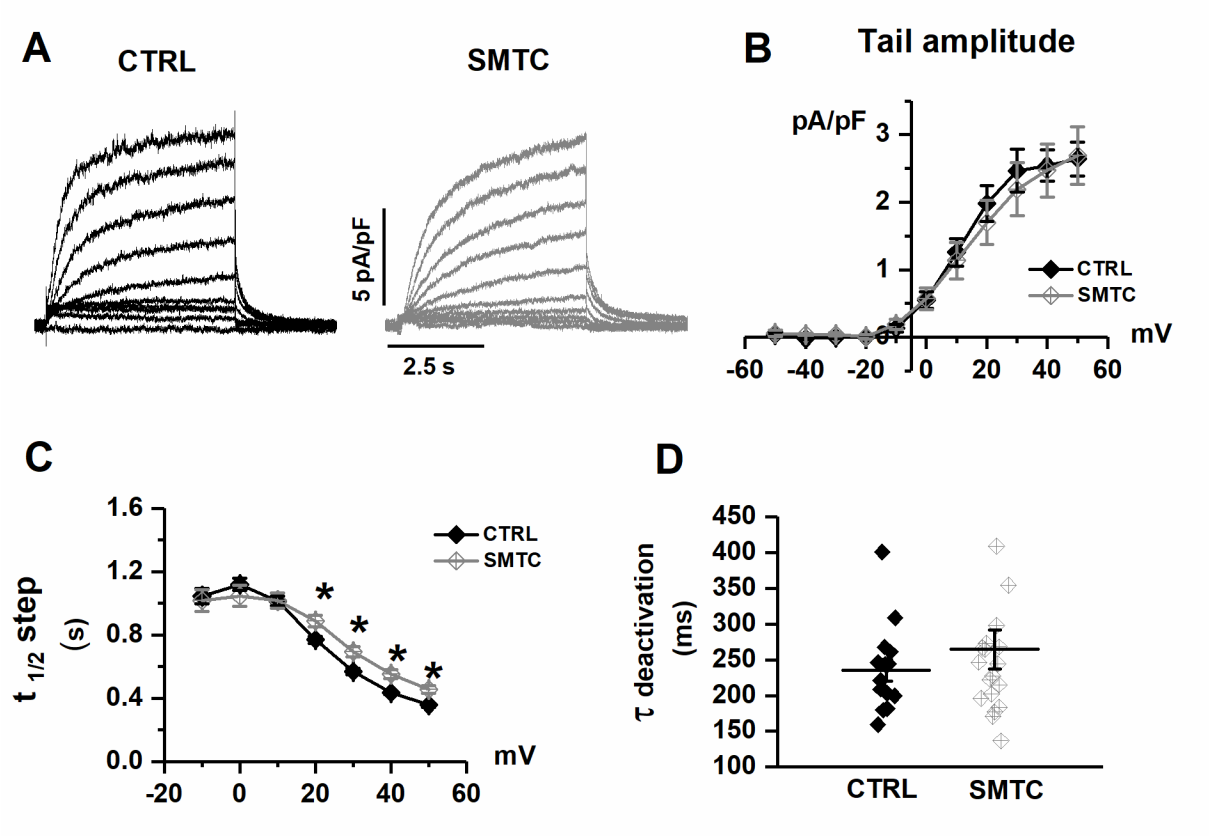

Figure S3. Effect of NOS1 inhibition on I_{Ks}. Data for CTRL and SMTC are presented in each panel. A) Records of I_{Ks} during step and tail at different step voltages; B) I/V relationship of I_{Ks} tail current; C) V-dependency of the time for half I_{Ks} activation ($t_{1/2}$) during the step; D) V-dependency (+40mV) of the time constant of I_{Ks} deactivation (τ) during the tail current. Sample sizes: CTRL n=16/7, SMTC n=19/6 for all panels. *=*P*<0.05 vs CTRL. From two-way ANOVA for repeated measurements.

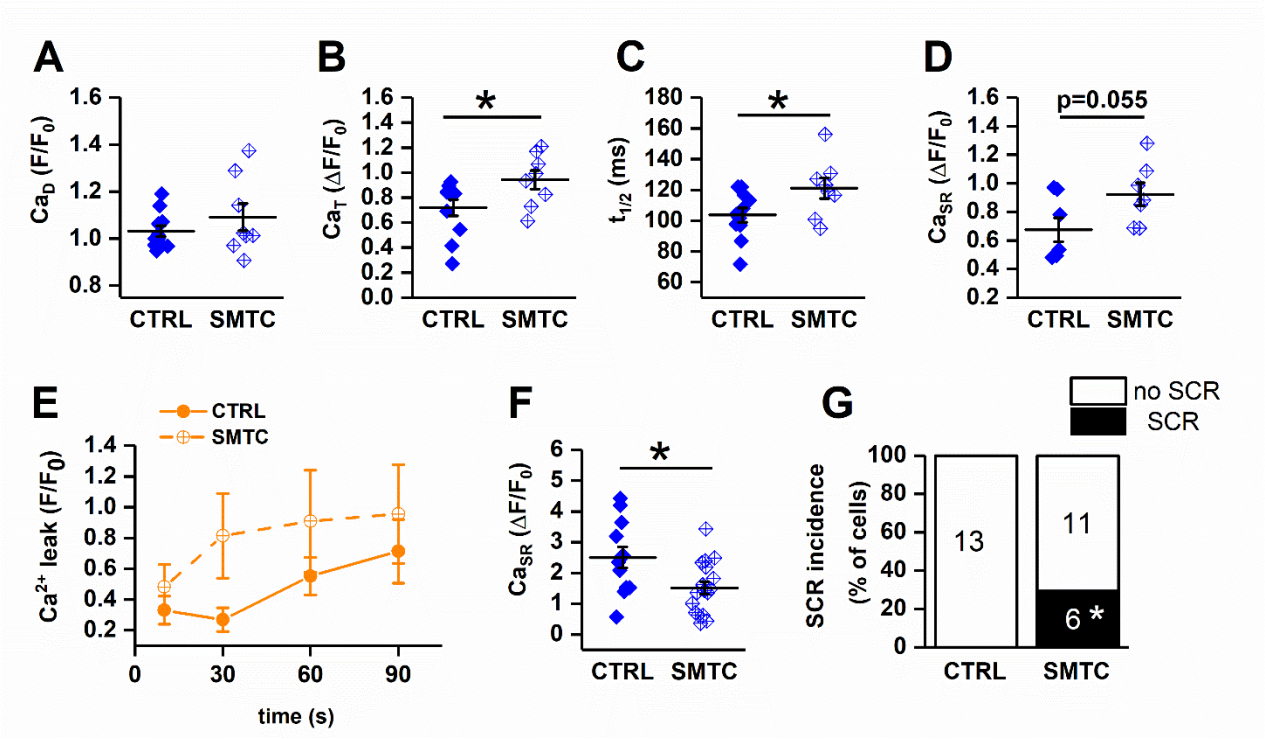

Figure S4. Effect of NOS1 inhibition on Ca^{2+} dynamics in GP myocytes. *Upper panels:* I-clamp recordings. SMTC-induced changes in diastolic Ca^{2+} (Ca_D, A), Ca^{2+} transient amplitude (Ca_T, B), half-time of Ca^{2+} decay ($t_{1/2}$, C) and SR Ca^{2+} content (Ca_{SR} D). These results refer to myocytes in which SCR did not occur. *Lower panels:* field stimulation recordings. SMTC-induced changes in tetracaine-sensitive Ca^{2+} leak (E), Ca_{SR} (F), and SCR incidence (G). Sample sizes: CTRL n=7/2, SMTC n=7/2 for panels A-D; CTRL n=13/4, SMTC n=17/3for panels E-G. *=*P*<0.05 vs CTRL from unpaired Student's test and chi squared test.

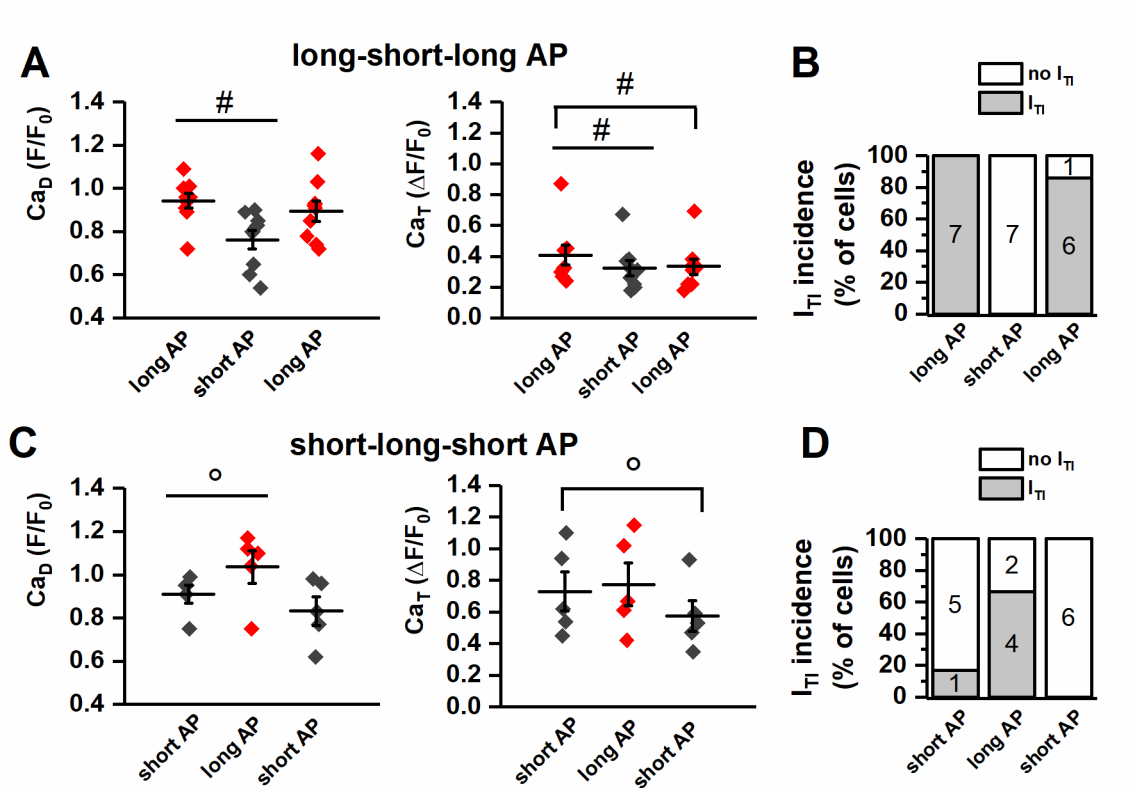

Figure S5. Reproducibility of APD effect on Ca^{2+} transient parameters. Changes in diastolic Ca^{2+} (Ca_D), Ca^{2+} transient amplitude (Ca_T) (panels A and C) and I_{TI} incidence (panels B and D) caused by change in AP waveform, in the long-short-long sequence (upper) or short-long-short one (lower). In the former sequence, only cells initially displaying I_{TI} events were considered (I_{TI} incidence = 100% in the first long AP trial). Sample sizes: n=7/4 for A and B; n=6/2 for C and D. #=*P*<0.05 vs long AP; °=*P*<0.05 vs short AP from two-way ANOVA for repeated measurements.

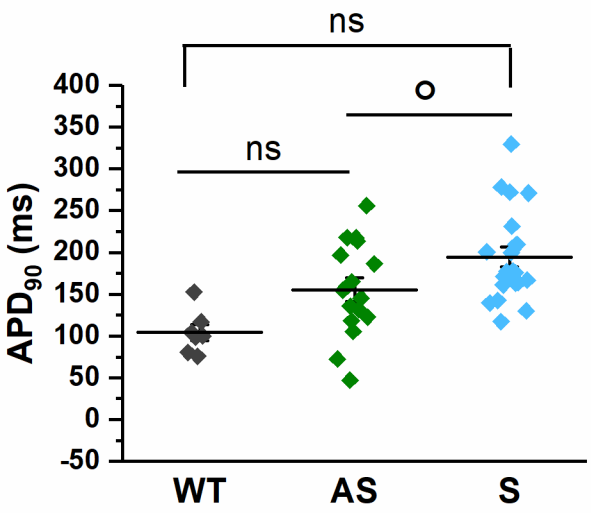

Figure S6. Effect of KLVQT1 mutation and SNP variant on APD in hiPSC-CMs. For clarity, only the data obtained under dynamic-clamp (DC) conditions are shown; similar results were obtained in the absence of DC. Comparison of APD_{90} between S KVLQT1-mutant (minor NOS1AP SNP), WT (minor NOS1AP SNP) and AS KVLQT1-mutant (major NOS1AP SNP). Sample sizes: S n=21/7, WT n=7/3. AS n=16/6. °=*P*<0.05 vs S from unpaired Student's test.

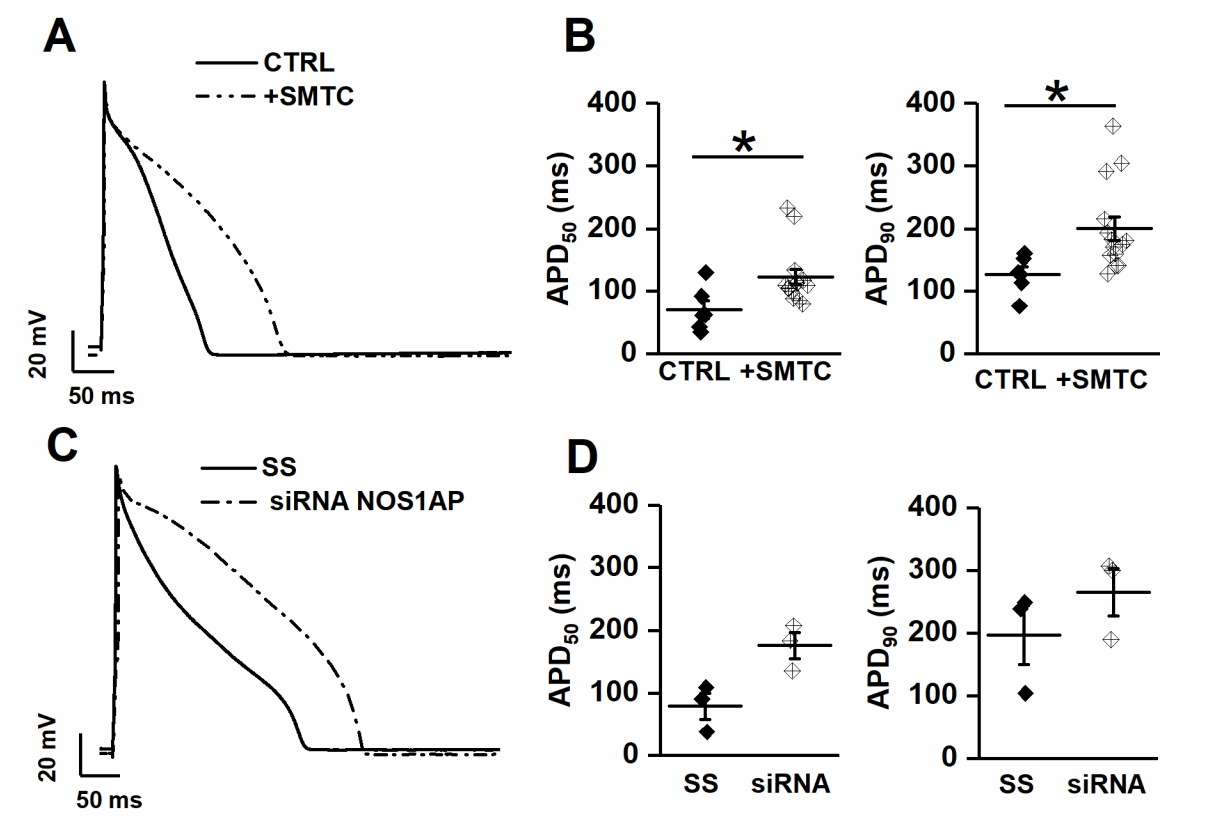

Figure S7. Effect of NOS1AP-dependent signaling on APD in WT hiPS-CMs carrying the major NOS1AP SNP. *Upper panels (A,B):* effect of NOS1AP knock-down (scramble sequence, SS solid line; siRNA, dotted line) on AP contour, APD_{50} and APD_{90}; *Lower panels (C,D)*: effect of NOS1 inhibition (control CTRL solid line, +SMTC, dotted line) on AP contour, APD_{50} and APD_{90} . Sample sizes: upper panels SS n= 3/1; siRNA n=3/1; lower panels CTRL n= 15/4; +SMTC n=15/4; *= P<0.05 vs CTRL from unpaired Student's test (calculated only if n>5).

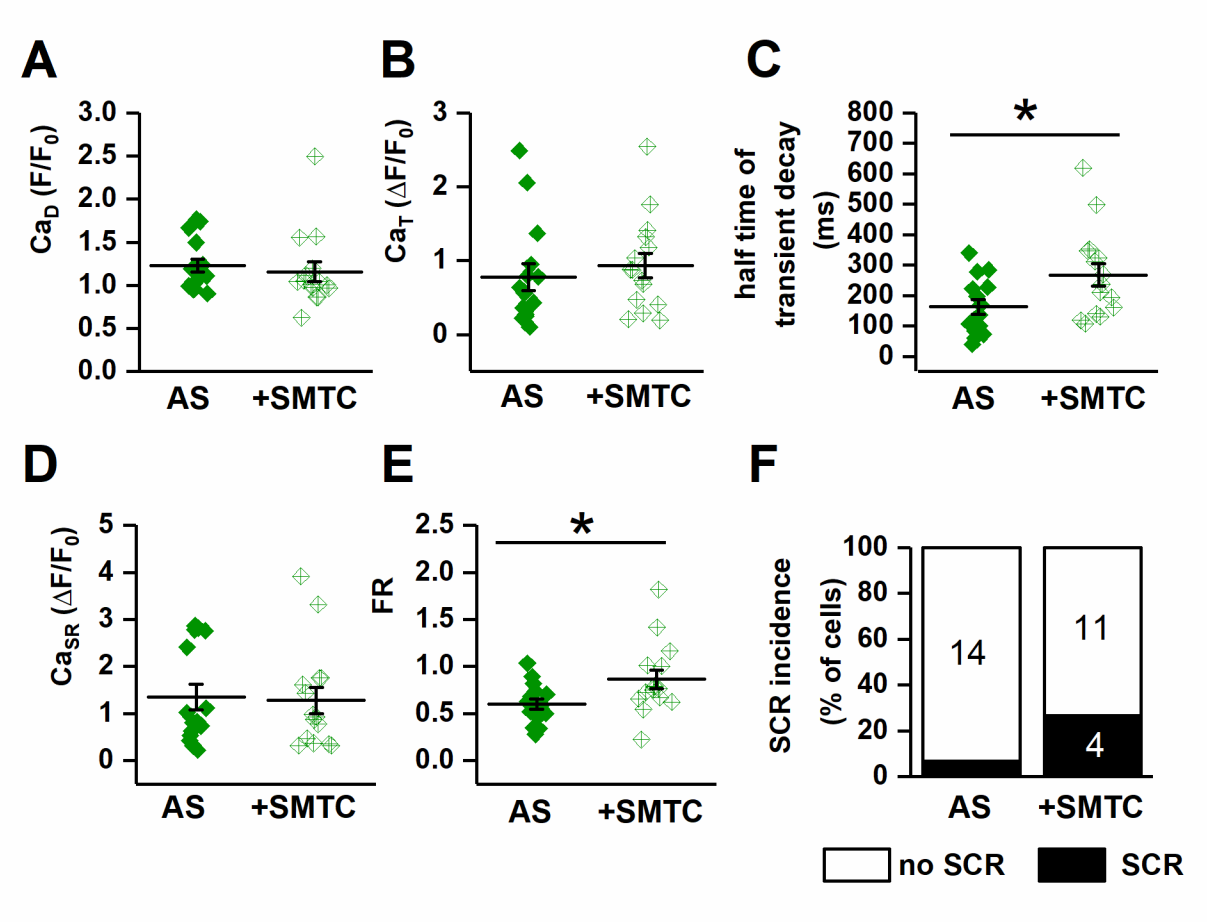

Figure S8. Effect of NOS1 inhibition on Ca^{2+} dynamics in KLVQT1-mutant AS hiPS-CMs (carrying the major SNP). Field-stimulation recordings. SMTC-induced changes in diastolic Ca^{2+} (Ca_D, A), Ca^{2+} transient amplitude (Ca_T, B), half-time of Ca^{2+} decay ($t_{1/2}$, C), SR Ca^{2+} content (Ca_{SR} D), fractional SR release (FR, E) and SCR incidence (F). Sample sizes: AS n= 14/4; +SMTC n=15/4. *= *P*<0.05 vs AS from unpaired Student's test.

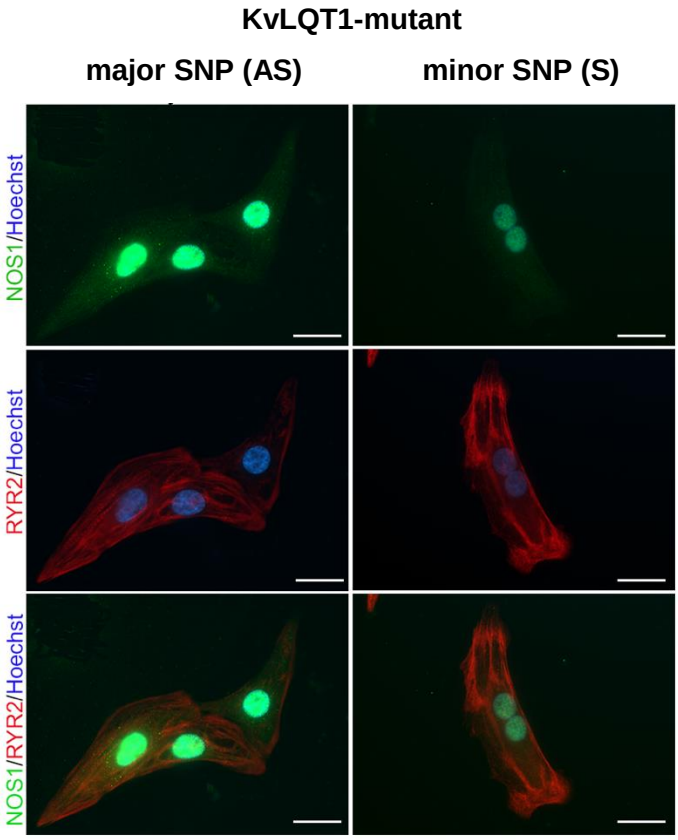

Figure S9. NOS1 expression and localization in KvLQT1-mutant hiPSC-CMs carrying the major or minor NOS1AP SNPs respectively. KvLQT1-mutant hiPSC-CMs carrying the major (left) and minor (right) NOS1AP alleles respectively were stained for NOS1 protein (green, upper panels), RyR2 protein (red, middle panel). NOS1-RyR2 overlap images (bottom panels). Nuclei in blue (Hoechst). Scale bars 20 µm.

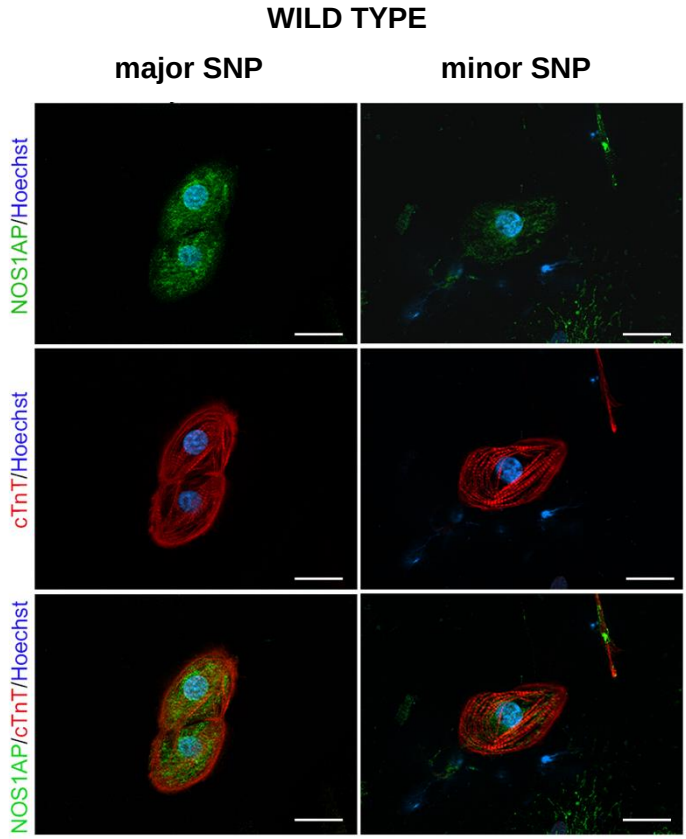

Figure S10. NOS1AP expression and localization in WT hiPS-CMs carrying the major or minor NOS1AP SNPs respectively. WT hiPS-CMs carrying the major (left) and minor (right) NOS1AP alleles respectively were generated and studied. Immunofluorescence staining of the same field for NOS1AP protein (green, upper panels, cardiac sarcomeric protein troponin T (red, middle panel). NOS1AP-CTnT overlap images (bottom panels). Nuclei in blue (Hoechst). Scale bars 20 µm.

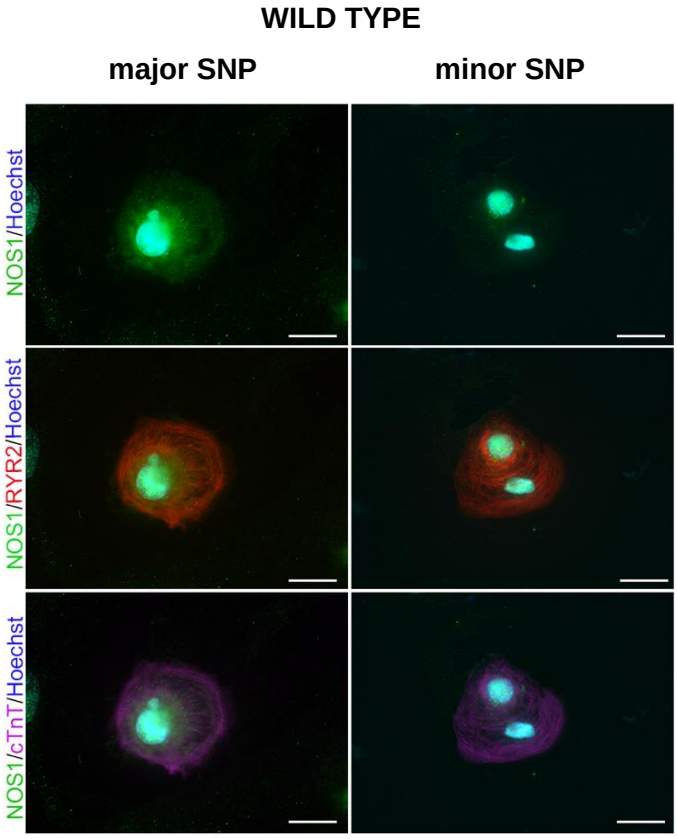

Figure S11. NOS1 expression and localization in WT hiPS-CMs carrying the minor or major NOS1AP SNPs respectively. WT hiPS-CMs carrying the major (left) and minor (right) NOS1AP alleles respectively were generated and studied. Immunofluorescence staining of the same field for NOS1 protein (green, upper panels), NOS1-RyR2 overlap image (RyR2 red, middle panel). NOS1-cTnT overlap images (cTnT purple, bottom panels). Nuclei in blue (Hoechst). Scale bars 20 µm.

SUPPLEMENT TABLES

Patient	Gender	Age at enrollment	Clinical history
S	Female	64	Symptomatic for syncope from the age of 16. Triggers for cardiac events: emotion and exercise. One cardiac arrest requiring DC shock at age of 35, β-blocker therapy (propranolol 40 mg x3) started; no more events since therapy initiation. ECG at age of 52 (β-blocker wash out): QT 500 ms, RR 710 ms; QTc 593 ms, HR 84 bpm
AS	Female	53	Daughter died at age of 12 while ice-skating after many misdiagnosed syncopes. The patient never had symptoms and was never on therapy. ECG at age 42: QT 452 ms, RR 860 ms; QTc 488, HR 69 bpm.

Table S1. Clinical parameters of hiPSC-CMs donors.

I_{CaL} parameters	CTRL	SMTC
peak current density (pA/pF)	-13.5 ± 1.0	-16.6 ± 1.2*
g_{max} (nS/pF)	0.29 ± 0.02	0.35 ± 0.02*
E_{rev} (mV)	60.3 ± 0.9	62.2 ± 1.0
$V_{0.5}$ A (mV)	-3.6 ± 0.7	-3.9 ± 0.5
A slope (mV)	7.0 ± 0.1	6.9 ± 0.1
$V_{0.5}$ I (mV)	-23.8 ± 1.0	-22.1 ± 0.6
I slope (mV)	4.8 ± 0.5	4.4 ± 0.2
I_{Kr} parameters	**CTRL**	**SMTC**
I_{max} (pA/pF)	0.98 ± 0.05	0.89 ± 0.04
$V_{0.5}$ A (mV)	-10.6 ± 1.3	-10.9 ± 1.2
A slope (mV)	5.4 ± 0.3	5.3 ± 0.4
I_{Ks} parameters	**CTRL**	**SMTC**
I_{max} (pA/pF)	2.94 ± 0.3	2.78 ± 0.4
$V_{0.5}$ A (mV)	14.4 ± 1.1	16.9 ± 1.7
A slope (mV)	8.6 ± 0.5	9.4 ± 0.6
τ deactivation (ms)	235.6 ± 15.5	261.9 ± 25.8

Table S2. Current (I_{CaL}, I_{Kr} and I_{Ks}) parameters in CTRL and SMTC treated GP myocytes. g_{max} = normalized maximal conductance; E_{rev} = reversal potential; $V_{0.5}$ A = voltage of half-maximal activation; A slope = slope factor (mV) of activation $V_{0.5}$ I = voltage of half-maximal inactivation; I slope = slope factor (mV) of inactivation; τ deactivation = time constant of tail current deactivation. *P<0.05 vs CTRL.

	Native		Dynamic Clamp (DC)	
	AS	**S**	**AS**	**S**
E_{diast} (mV)	-40.2 ± 11.5	-38.7 ± 4.7	-75.2 ± 3.4	-76.3 ± 1.08
APA (mV)	40.9 ± 4.9	47.1 ± 5.2	39.8 ± 7.2	52.2 ± 3.1*
APD_{90} (ms)	109.5 ± 27.5	169.6 ± 34.8*	135.5 ± 35.9	196.2 ± 33.03*
APD_{50} (ms)	79.6 ± 22.4	131.9 ± 39.3*	92.1 ± 29.2	142.3 ± 30.7*
APD_{20} (ms)	45.6 ± 13.3	73.3 ± 18.6*	46.7 ± 18.6	76.2 ± 28.9
ADP_{90}/ADP_{50}	1.4 ± 0.1	1.3 ± 0.07	1.5 ± 0.17	1.4 ± 0.13

Table S3. AP parameters in S and AS hiPSC-CMs under native and Dynamic Clamp conditions. E_{diast} = diastolic potential; APA = action potential amplitude; APD_x= action potential duration at the indicated repolarization level (%). (S nat n=13 AS nat n=11, S DC n=16, AS DC n=13). *=*P*<0.05 vs AS.

I_{CaL} Parameters	**S**	**AS**
Peak density (pA/pF)	-29.8 ± 4.4 *	-16.7 ± 2.0
g_{max} (nS/pF)	0.8 ± 0.1	0.45 ± 0.04
E_{rev} (mV)	57.5 ± 3.8	52.5 ± 3.0
$V_{0.5}$ A(mV)	-4.8 ± 1.6	-4.4 ± 1.2
A slope (mV)	6.7 ± 0.3	7.1 ± 0.31
$V_{0.5}$ I (mV)	-31.4 ± 1.9	-31.3 ± 1.8
I slope (mV)	5.4 ± 0.5	5.0 ± 0.1

Table S4. I_{CaL} parameters in S vs AS hiPSC-CMs. g_{max} = normalized maximal conductance; E_{rev} = reversal potential; Act $V_{0.5}$ A = voltage of half-maximal activation; A slope = slope factor (mV) of activation; $V_{0.5}$ I = voltage of half-maximal inactivation; I slope = slope factor (mV) of inactivation. (AS n=10, S n=12). *=*P*<0.05 vs AS.

SUPPLEMENTAL RESULTS

Guinea-pig experiments

Effect of NOS1 inhibition by L-VNIO on repolarization and DADs occurrence

To rule out that the observations resulted from SMTC effect other than NOS1 inhibition (ancillary effects), experiments were repeated using a different NOS1 inhibitor, L-VNIO (100 μM). This concentration was selected because previously shown to mimic the effect of NOS1 gene knock-out in murine ventricular myocytes [1]. The experiments were performed on a background of I_{Ks} blockade plus 1 or 10 nM ISO.

L-VNIO significantly prolonged APD (73.3 ± 2.9 vs 94.3 ± 10.1 ms; $P<0.05$). The lower ISO concentration induced DADs in none of 11 CTRL myocytes and in 6 of 9 L-VNIO treated myocytes (0% vs 66.7%; $P<0.01$. **Figure S1A**). At the higher ISO concentration DADs occurred in 100% of both CTRL and L-VNIO treated myocytes (**Figure S1B**); however, the time of DADs occurrence was significantly shorter in L-VNIO than in CTRL (**Figure S1C**). Furthermore, at the higher ISO concentration, DADs occasionally (4 of 9 cells) resulted in triggered activity in L-VNIO but never in CTRL ($P<0.01$ vs CTRL. **Figure S1D**). L-VNIO effect was fully consistent with that of SMTC (reported in the manuscript).

Effect of NOS1 inhibition by SMTC on membrane currents I_{Kr} and I_{Ks}

While I_{CaL} modulation by SMTC is illustrated in a manuscript figure (**Figure 3**), I_{Kr} and I_{Ks} modulation was minor and probably irrelevant to the effect of NOS1 inhibition on repolarization; therefore, the respective figures are shown here only.

I_{Kr} maximal conductance, steady-state activation parameters and rectification ratio (reflecting channel inactivation) were not affected by NOS1 inhibition (**Figure S2 and Table S2**).

I_{Ks} density, maximal conductance and steady-state activation parameters were similarly unaffected by NOS1 inhibition (**Figure S3A**-**B**, **Table S2**). The $t_{1/2}$ for I_{Ks} activation was slightly but significantly prolonged by NOS1 inhibition (**Figure S3C**). Deactivation kinetics was well fitted by a single exponential, whose time constant (τ) was not affected by NOS1 inhibition (**Figure S3D and Table S2**).

Overall, NOS1 inhibition did not affect I_{Kr} and moderately slowed I_{Ks} activation. The observation that the effect of I_{Ks} blockade on APD was similar in SMTC-treated and CTRL cardiomyocytes (**Figure 1C**) suggests that I_{Ks} modulation was unlikely to account for APD prolongation induced by NOS1 inhibition.

Effect of NOS1 inhibition by SMTC on intracellular Ca^{2+} dynamics

Intracellular Ca^{2+} dynamics was measured in patched myocytes under I-clamp conditions (APD free to change). SMTC did not affect diastolic Ca^{2+} (**Fig S4A**), increased Ca_T amplitude (**Fig S4B),** slowed Ca^{2+} decay (**Fig S4C**) and tended to increase SR Ca^{2+} content (**Fig S4D).**

Tetracaine-sensitive SR Ca^{2+} leak, SR Ca^{2+} content after the leak period and the incidence of spontaneous Ca^{2+} release events (SCR) were measured under field-stimulation (no dialysis, APD free to change). SMTC increased Ca^{2+} leak (**Fig S4E),** as also indicated by the reduced SR Ca^{2+} content at the end of the leak period (**Fig S4F**). Under field stimulation, SMTC increased the incidence of SCR events (**Fig S4G**).

Effect of APD on intracellular Ca^{2+} and I_{TI} occurrence: reproducibility with different waveform sequences

To rule out dependency of intracellular Ca^{2+} parameters on the order of waveforms sequence, the latter was inverted in a subset of experiments. Irrespective of the waveform sequence, Ca_D was consistently higher under the longer AP; as above, the response of Ca_T was less consistent, in a way again compatible with I_{CaL} run down (**Figure S5**).

hiPSC-CMs experiments:

Comparison of AP parameters between native and DC conditions

Action potential parameters of AS and S hiPSC-CMs are reported for native and DC conditions in **Table S3**.

Under native conditions hiPSC-CMs displayed a depolarized and unstable diastolic potential, which often resulted in automatic activity (see manuscript **Figure 5**). The majority of cells had a ventricular-like AP contour (see criteria in Methods) for both S and AS groups; cells with other contours were discarded. Whereas diastolic potential was similar between S and AS hiPSC-CMs, APD was significantly longer in S than in AS hiPSC-CMs, also under native conditions (**Figure 5**).

I_{K1} injection by DC hyperpolarized diastolic potential to -80 mV (the target potential in setting I_{K1} conductance value), abolished automatic activity and prolonged APD. Since I_{K1} is an outward current, APD prolongation must be the consequence of dependency of currents other than I_{K1} on diastolic potential. The difference in APD between S and AS hiPSC-CMs was preserved under DC conditions.

Interaction between KvLQT1 mutation and NOS1AP SNPs in affecting APD

To assess the interaction between the KvLQT1 mutation and NOS1AP minor allele in prolonging repolarization, APD was compared between KvLQT1 mutant hiPSC-CMs (AS and S) and WT hiPSC-CMs (from the same population) harboring the minor NOS1AP allele (**Figure S6**). Among hiPS-CMs carrying the minor NOS1AP allele, the KvLQT1 mutation was associated with longer APD; however, APD was similar between KvLQT1-mutant hiPS-CMs carrying the major NOS1AP allele and WT ones carrying the minor NOS1AP allele. Thus, the APD difference caused by the KvLQT1mutation was “compensated” by expression of the major NOS1AP allele. However, because of the small size of the WT sample, this result has to be interpreted with caution.

Comparison of I_{CaL} parameters between S and AS cells

I_{CaL} in S and AS hiPSC-CMs is compared in manuscript **Figure 6**. I_{CaL} parameters measured in those experiments are summarized in **Table S4**.

Effect of NOS1 inhibition by SMTC on intracellular Ca^{2+} dynamics

Intracellular Ca^{2+} dynamics and SCR incidence were measured in unpatched hiPS-CMs under field stimulation (no dialysis, APD free to change). SMTC slowed Ca^{2+} decay ($t_{1/2}$, **Figure S8C**) and increased fractional Ca^{2+} release (FR, **Figure S8E**), but failed to affect the remaining parameters.

Molecular characterization

To test the effect of NOS1AP variants independently of KvLQT1 mutation, NOS1 expression and its colocalization with RyRs and cTNT was compared between different NOS1AP alleles in WT hiPSC-CMs from two unrelated populations (**Figure S10**). Also in WT hiPSC-CMs the minor NOS1AP allele was associated to reduced NOS1 expression and with its reduced colocalization with RyRs and cTnT (**Figure S11**).

SUPPLEMENT METHODS

Experimental Models

Guinea pig (GP) ventricular myocytes

Dunkin-Hartley GP were euthanized by cervical dislocation under anesthesia with zolazepam + tiletamine (Telazol 100 mg/Kg i.p.). Ventricular cardiomyocytes were enzymatically dissociated by using a retrograde coronary perfusion method previously published 21, with minor modifications. Rod-shaped, Ca^{2+} -tolerant cardiomyocytes were used within 12 hours from dissociation. All experiments conformed to the guidelines for Animal Care endorsed by the University of Milano-Bicocca. A total of 15 animals were used.
To reproduce the LQT1 phenotype we subjected GP ventricular cardiomyocytes to I_{Ks} blockade (2μM JNJ303) and adrenergic stimulation (Isoproterenol, ISO 1 nM). In these cells we measured electrical activity, membrane currents and intracellular Ca^{2+} dynamics, in basal condition (CTRL group) and under selective inhibition of NOS1 activity by incubation with 3μM S-methyl-L-thiocitrulline (SMTC) [2] for at least 30 minutes (SMTC group). As a confirmation, for some experiments we also used another NOS1 inhibitor, Vynil-L-NIO (L-VNIO) [3]. NOS1 inhibitors were added both in the perfusion solution and dialyzed into the cell through the patch pipette.

hiPSC-CMs preparation

hiPSC were generated and characterized as previously described [4, 5]. The reprogramming protocol is briefly summarized here

Features of S and AS hiPSC-CMs donors
The clinical features of the KCNQ1 mutation carriers from which hiPSC-CMs were obtained are reported in **Table S1**.

Cell culture
Human dermal fibroblasts (HDFs), mouse embryonic fibroblasts (MEFs), and 293T were cultured in HDF medium composed of Dulbecco Modified Eagle Medium (DMEM), 10% Fetal Bovine Serum (FBS), 2mM L-glutamine, 50 U/ml penicillin, 50 U/ml streptomycin, 1% Non Essential Amminoacid (NEAA). Human induced pluripotent stem cells (hiPSCs) were maintained on irradiated MEF in human embryonic stem cell (hESC) medium composed of DMEM-F12, 20% KnockOut serum replacement (KO-SR), 10 ng/ml basic fibroblast growth factor (bFGF), 1 mM-glutamine, 1% NEAA, 50 U/ml penicillin, 50 U/ml streptomycin, and 0.1 mM 2-mercaptoethanol.

Retrovirus preparation
293T packaging cells were co-transfected with each of the 4 retroviral vectors encoding for human OCT4, SOX2, KLF4 and cMYC (Addgene), and with the packaging vector pCL-Eco (Addgene), using the calcium/phosphate method. The viral particles released in the medium were collected, filtered with 0.45 μm PVDF filters and immediately used to infect HDFs.

Generation of hiPSCs
HDFs were transduced with a mix of the 4 retroviruses in two consecutive rounds of infection, in the presence of 4 μg/ml polybrene (Sigma Aldrich). 6 days after transduction, HDFs were harvested and re-plated onto MEF feeders in hESC medium. 24 days after infection, the emerging hiPSC clones were mechanically isolated.

Embryoid body formation and three germ layer differentiation in vitro
hiPSCs were grown for 7 days in non-adherent conditions in a modified hESC medium deprived of bFGF, and containing 20% FBS in place of KO-SR. Forming embryoid bodies (EBs) were then transferred to gelatin-coated dishes to allow differentiation for other 7 days in adhesion. Three germ layer formation was assessed by immunocytochemistry.

Genotyping

Genomic DNA was extracted from hiPSCs using the QIAmp DNA Blood Mini kit (Qiagen) according to the manufacturer's instructions. The regions of interest on KCNQ1 and NOS1AP genes were amplified by PCR using specific primers, and then sequenced (Lightrun service - GATC Biotech AG-Germany; www.gatc-biotech.com/lightrun).

Karyotyping

hiPSCs were blocked at metaphase by exposure for 3 hours to 10 µg/ml demecolcine solution. Karyotype analysis was performed using G-banding chromosome analysis, according to standard procedures (International System for Human Cytogenetic Nomenclature 2013).

Alkaline phosphatase colorimetric assay

Alkaline phosphatase (AP) colorimetric assay was performed on hiPSCs seeded on feeders in 24-multiwells using the Alkaline Phosphatase Staining kit (Stemgent) and following manufacturer's instructions.

Differentiation into cardiomyocytes (CMs)

hiPSCs were differentiated into CMs with the PSC Cardiomyocyte Differentiation Kit (ThermoFisher). Contracting hiPSC-CMs appeared as early as 11 days after the initiation of the differentiation protocol. hiPSC-CMs were characterized by RT-PCR and immunofluorescence for cardiac-specific proteins at different time points.

Dissociation of contracting EBs

Spontaneously contracting EBs were micro-sectioned, dissociated with 1 mg/ml collagenase B at 37°C for 40 minutes, and adhered onto gelatin-coated dishes or glass slides.

Electrophysiology

The baseline solution for all patch-clamp recordings was standard Tyrode's solution containing (mM): 154 NaCl, 4 KCl, 2 $CaCl_2$, 1 $MgCl_2$, 5 HEPES-NaOH, 5.5 D-glucose, adjusted to pH 7.35 with NaOH. Membrane capacitance and series resistance were measured and automatically compensated in every cell. Signals were acquired with a MultiClamp 700B amplifier (Axon Instrument), connected to a Digidata 1440A (Molecular Devices) and filtered with an appropriate Bessel filter via pClamp 10 (Molecular Devices). All measurements were performed at 36.5°C.

I-clamp and Dynamic Clamp recordings

Membrane potential was recorded during steady-state pacing at a cycle length of 2 Hz for GP cardiomyocytes and 1 Hz for hiPSC-CMs.

Cells were patch-clamped with borosilicate glass pipettes containing (mM): K^+-aspartate 110, KCl 23, $MgCl_2$ 3, HEPES KOH 5, EGTA KOH 0.1, GTP Na^+-salt 0.4, ATP Na^+-salt 5, creatine phosphate Na^+-salt 5, $CaCl_2$ 0.04 (calculated free-Ca^{2+} = 10^{-7} M), adjusted to pH 7.3. Series resistance was <5 MΩ and was compensated to 80% of its value.

In hiPSC-CMs, "synthetic" I_{K1} was injected by the dynamic-clamp (DC) technique to correct for low endogenous I_{K1} expression. I_{K1} conductance required to achieve a diastolic potential (Ediast) around -80 mV was 1.9 nS/µF (kept constant in all cells); this abolished automatic activity and resulted in physiological AP contours (examples in manuscript **Figure 5**). hiPSC-CMs with ventricular-like APs were selected based on an APD90/APD50 ratio lower than 2 (under DC conditions), as previously reported [6, 7]. The following parameters were considered: AP duration at 90% repolarization (APD90, measured beat by beat by an automated routine); incidence and time of occurrence of afterdepolarizations (EADs and DADs), defined as transient membrane depolarizations > 0.5 mV occurring before and after AP repolarization respectively [8]. "Triggered activity", observed in hiPSC-CMs only, was defined as APs arising from afterdepolarizations; it was distinguished from "automaticity" because of the absence of a proper diastolic depolarization phase (**Figure S1**).

Only cells in which DC successfully polarized diastolic potential were used. Synthetic I_{K1} was

generated by a human numerical current model derived from Rudy-O'Hara one [9] and injected in the cell using the Real-Time eXperiment Interface (RTXI) as previously described [10]. I_{K1} conductance was set to achieve a diastolic potential (E_{diast}) around -80 mV; the value of I_{K1} conductance was the same in all cells.

Standard V-clamp experiments

I_{CaL} was isolated by using a Na^+- and K^+-free extracellular solution, in which the two ions were replaced, containing (mM): 154 tetraethylammonium chloride (TEACl), 1 $MgCl_2$, 2 $CaCl_2$, 5 HEPES, 5.5 D-glucose, with pH adjusted to 7.4 with TEAOH. Intracellular solution contained (mM): 115 CsCl, 20 TEACl, 0.5 $MgCl_2$, 10 EGTA CsOH, 5 HEPES CsOH, 5 ATP Mg^{2+}-salt, 5 creatine phosphate Tris-salt, 0.4 GTP Tris-salt; at pH 7.2 with CsOH. For I_{CaL} recordings in hiPSC-CMs, extracellular $CaCl_2$ and D-glucose were elevated to 5 mM and 10 mM respectively; 2 mM 4-aminopyridine (4-AP) and 10 µM tetrodotoxin (TTX) were added. To construct peak I/V relationships, I_{CaL} was elicited by 300 ms steps (range -50 to +60 mV) from a holding potential of -40 mV. Activation and inactivation curves were obtained from peak current I/V relationship and fitted with Boltzmann functions to extract gating parameters. The latter included voltage of half-maximal activation/inactivation ($V_{0.5}$, mV), slope factor (k, mV), maximal conductance (g_{max}, nS). Series resistance was compensated up to 80% to minimize voltage error.

I_{NaL} was measured under AP-clamp (see below) and dissected as the current sensitive to 1µM TTX. A representative AP, recorded under NOS1 inhibition (by SMTC), was used as the command signal. The measurement was performed during Tyrode's superfusion (see above), with pipette solution containing 0.1mM EGTA.

I_{Ks} and I_{Kr} were isolated by subtraction, as currents sensitive to their specific blockers JNJ303 (2 µM) and E-4031 (5 µM) respectively. Pipette solution contained (mM): 110 K^+-aspartate, 23 KCl, 3 $MgCl_2$, 2 $CaCl_2$, 5 HEPES-KOH, 5 EGTA-KOH, 5 ATP Na^+-salt, 5 creatine phosphate Na^+-salt, 0.4 GTP Na^+-salt, pH adjusted to 7.3 with KOH. 5 µM nifedipine was added to rule out interference by I_{CaL}. From a holding potential of -40 mV, depolarizing steps (range -50 to +50 mV) of 5s for I_{Ks} and of 1 s for I_{Kr} were applied (interpulse interval was 11 s for I_{Ks} and 3 s for I_{Kr}). I_{Ks} amplitude was measured as peak current occurring upon returning to holding potential ("tail current" amplitude). I_{Kr} was measured at the end of the activating step and as tail current; the "rectification ratio", which reflects channel inactivation, was estimated from the ratio between the step and tail current amplitudes. The time-course of changes was described by the time constant (τ) of monoexponential fitting, or by the time to half-maximal transition ($t_{1/2}$) when monoexponential fitting was inadequate.

Action-potential clamp (AP-Clamp) experiments

Short (APD_{90} = 100 ms) and long (APD_{90} = 140 ms) AP waveforms were selected from previous I-clamp recordings in control and during NOS1 inhibition respectively. Their APD_{90} differed by a proportion (40%) roughly representative of clinically observable QT prolongation. The AP waveforms were applied as "command potential" in V-clamp mode at the same rate at which they were recorded (2 Hz for both AP waveforms); thus, the longer AP was associated with a shorter diastolic interval. Because the AP waveforms were not obtained from the same myocyte in which they were applied, membrane current was not null during the AP and was disregarded. The relevant parameter in these experiments was the occurrence of inward current transients (I_{TI}) during diastole, assumed to reflect the occurrence of intracellular Ca^{2+} waves, a sign of SR instability. I_{TI} events were defined as inward I fluctuations exceeding a threshold of -15 pA (>2 SD of baseline current); the proportion of cells in which at least 1 I_{TI} event occurred was measured to obtain I_{TI} incidence. Furthermore, the number of I_{TI} events within each cycle, the time of onset of the earliest event and the I_{TI} integral (representative of charge flowing in each event) were considered. Measurements were carried out under superfusion with 1 nM isoproterenol (ISO) to simulate conditions of arrhythmia occurrence in LQTS. In general, the long AP was applied first and, when I_{TI} events were stably detected, V-clamp was continued, within the same myocyte, with short AP. Nevertheless, to rule out time as a cause of changes in I_{TI} occurrence, in preliminary experiments a long-long sequence of APs, with each phase lasting > 15 seconds, was applied. This did not result in changes of I_{TI} occurrence (n= 7). Furthermore, in myocytes in which long-

short-long sequences could be applied, I_{TI} suppression by short AP was reversed by switching back to long AP in 7/8 cells (**Figure S5**).

Intracellular Ca^{2+} recordings

Guinea pig ventricular myocytes were incubated for 30 minutes in 10 µM Fluo4-AM and washed. The dye was excited at a wavelength of 494 nm and emission was collected through a 535 nm band pass filter. Light emission was amplified, converted to voltage, low-pass filtered (200 Hz) and digitized at 2 kHz. Background luminescence was recorded from a cell free field and subtracted; the fluorescence signal recorded from the cell in the quiescent state (before any intervention) was used as reference fluorescence (F_0) for signal normalization (F/F_0). Intracellular Ca^{2+} was expressed in F/F_0 units.

The amplitude of V-triggered Ca^{2+} transients (Ca_T) was measured as the difference between diastolic Ca^{2+} (Ca_D) and Ca_T peak; the half time of Ca_T decay ($t_{1/2}$) was measured after estimating the decay asymptote by mono-exponential fitting; SR Ca^{2+} content (Ca_{SR}) was measured as the amplitude of the caffeine-induced (10 mM, 5 s) Ca^{2+} transient; fractional release (FR) was calculated as the Ca_T/Ca_{SR} ratio. To evaluate Ca^{2+} leak through RyR2 channels, cells were field-stimulated (2Hz) to steady-state Ca_T; stimulation was then discontinued and Ca^{2+} bild-up was measured in the presence of Na^+/Ca^{2+} exchanger inhibition (Na^+- and Ca^{2+}-free superfusion). The protocol was then repeated in the same cell after exposure to tetracaine (0.1 mM) and tetracaine-sensitive Ca^{2+}-leak was estimated by subtraction (the control-tetracaine sequence was swapped in alternate cells to avoid systematic time-dependent artefact). Spontaneous Ca^{2+} release events (SCR) were defined as clearly identifiable (>1.5 of baseline) diastolic oscillations of the Ca^{2+} signal and their incidence expressed as % of cells in which they occurred.

To test the effect of changes in AP duration under control and NOS1 inhibition Ca^{2+} recordings were performed under AP-clamp (see above). In other experiments (as detailed in the results) intracellular Ca^{2+} was measured under I-clamp. Whenever measurements were likely affected by pipette dialysis (in hiPS-CMs, or when SR Ca^{2+} leak was measured), intracellular Ca^{2+} recordings were obtained during field-stimulation of un-patched cells.

Molecular studies

Reverse transcription, PCR and real Time qPCR

Total RNA was extracted from CMs using Trizol® Reagent (Invitrogen) according to the manufacturer's instructions, and used for cDNA synthesis with SuperScript IV Reverse Transcriptase (ThermoFisher). cDNA were amplified by PCR with Phire Green Hot Start II PCR Master Mix (ThermoFisher), or by Real Time PCR with Power SYBR Green PCR Master Mix (Applied Biosystems, Carlsbad, California, USA) and the ABI Prism 7900HT Fast Real Time PCR System (Applied Biosystems). Primers for PCR were designed by using the 'Primer3 input' software and the specificity of each primer was confirmed using the BLAST software (NCBI).

Western blot

Cells were lysed in ice-cold RIPA buffer supplemented with protease inhibitors. The extracted proteins were separated by sodium dodecyl sulphate polyacrylamide gel electrophoresis (SDS-PAGE), and then transferred onto nitrocellulose membrane by a Transblot Turbo (BioRad Laboratories, Hercules, CA, USA). For immunoblotting, membranes were blocked in Odyssey Blocking Buffer (Li-COR), and then incubated overnight at 4ºC with anti-CAPON (R-300) antibody (sc-9138, Santa Cruz Biotechnology) or anti-actin antibody (ab3280, Abcam) diluted in Odyssey Blocking Buffer. At the end of the incubation, membranes were washed in PBS 0.1% tween 20 and subsequently incubated for 1 hour with IRDYE 800-conjugated secondary antibody at room temperature. After further washes, bands were visualized with the Odyssey Infrared Imaging System (Li-COR).

Immunofluorescence

hiPSC-CMs were fixed in 4% paraformaldehyde for 15 minutes, rinsed 3 times in PBS, and permeabilized in 0.2% Triton X-100 for 5 minutes. Samples were blocked with 1% bovine serum albumin (BSA) for 1 hour. The cells were incubated for 1 hour at room temperature or overnight

at 4°C with antibody diluted in 1% BSA, and then rinsed 3 times for 5 minutes with PBS. Further incubation was performed with the appropriate secondary antibody for 60 minutes at room temperature. The cells were rinsed once more, counterstained with Hoechst 33258, and analyzed with the AxioObserver.Z1 (Zeiss, Oberkochen, Germany).

Duolink Proximity Ligation Assay (PLA)

The interaction between NOS1AP and NOS1 in hiPSC-CMs was detected using the Duolink In situ Orange Starter Kit Mouse/Rabbit (DUO92102, Sigma Aldrich) according to manufacturer's instructions. Primary antibody incubation against NOS1AP (sc-9138 rabbit antibody, Santa Cruz Biotechnology) and NOS1 (610309 mouse antibody, BD Transduction Laboratories) was performed using the same conditions as immunostaining. The cells were visualized using the AxioObserver Z1 (Zeiss, Oberkochen, Germany).

SUPPLEMENT REFERENCES

1. Zhang YH, Zhang MH, Sears CE, Emanuel K, Redwood C, El-Armouche A, Kranias EG and Casadei B. Reduced phospholamban phosphorylation is associated with impaired relaxation in left ventricular myocytes from neuronal NO synthase-deficient mice. *Circ Res*. 2008;102:242-9.
2. Cutler MJ, Plummer BN, Wan X, Sun QA, Hess D, Liu H, Deschenes I, Rosenbaum DS, Stamler JS and Laurita KR. Aberrant S-nitrosylation mediates calcium-triggered ventricular arrhythmia in the intact heart. *Proc Natl Acad Sci U S A*. 2012;109:18186-91.
3. Babu BR and Griffith OW. N5-(1-Imino-3-butenyl)-L-ornithine. A neuronal isoform selective mechanism-based inactivator of nitric oxide synthase. *J Biol Chem*. 1998;273:8882-9.
4. Mura M, Pisano F, Stefanello M, Ginevrino M, Boni M, Calabro F, Crotti L, Valente EM, Schwartz PJ, Brink PA and Gnecchi M. Generation of the human induced pluripotent stem cell (hiPSC) line PSMi007-A from a Long QT Syndrome type 1 patient carrier of two common variants in the NOS1AP gene. *Stem Cell Res*. 2019;36:101416.
5. Mura M, Pisano F, Stefanello M, Ginevrino M, Boni M, Calabro F, Crotti L, Valente EM, Schwartz PJ, Brink PA and Gnecchi M. Generation of two human induced pluripotent stem cell (hiPSC) lines from a long QT syndrome South African founder population. *Stem Cell Res*. 2019;39:101510.
6. Matsa E, Rajamohan D, Dick E, Young L, Mellor I, Staniforth A and Denning C. Drug evaluation in cardiomyocytes derived from human induced pluripotent stem cells carrying a long QT syndrome type 2 mutation. *Eur Heart J*. 2011;32:952-62.
7. Rajamohan D, Kalra S, Duc Hoang M, George V, Staniforth A, Russell H, Yang X and Denning C. Automated Electrophysiological and Pharmacological Evaluation of Human Pluripotent Stem Cell-Derived Cardiomyocytes. *Stem Cells Dev*. 2016;25:439-52.
8. Paavola J, Viitasalo M, Laitinen-Forsblom PJ, Pasternack M, Swan H, Tikkanen I, Toivonen L, Kontula K and Laine M. Mutant ryanodine receptors in catecholaminergic polymorphic ventricular tachycardia generate delayed afterdepolarizations due to increased propensity to Ca2+ waves. *Eur Heart J*. 2007;28:1135-42.
9. O'Hara T, Virag L, Varro A and Rudy Y. Simulation of the undiseased human cardiac ventricular action potential: model formulation and experimental validation. *PLoS Comput Biol*. 2011;7:e1002061.
10. Altomare C, Bartolucci C, Sala L, Bernardi J, Mostacciuolo G, Rocchetti M, Severi S and Zaza A. IKr Impact on Repolarization and Its Variability Assessed by Dynamic Clamp. *Circ Arrhythm Electrophysiol*. 2015;8:1265-75.